



LAWRENCE
LIVERMORE
NATIONAL
LABORATORY

Explicit integrators for the time-dependent Kohn-Sham equations within the plane-wave pseudopotential formalism

A. Schleife, E. Draeger, Y. Kanai, A. Correa

November 28, 2011

Journal of Chemical Physics

Disclaimer

This document was prepared as an account of work sponsored by an agency of the United States government. Neither the United States government nor Lawrence Livermore National Security, LLC, nor any of their employees makes any warranty, expressed or implied, or assumes any legal liability or responsibility for the accuracy, completeness, or usefulness of any information, apparatus, product, or process disclosed, or represents that its use would not infringe privately owned rights. Reference herein to any specific commercial product, process, or service by trade name, trademark, manufacturer, or otherwise does not necessarily constitute or imply its endorsement, recommendation, or favoring by the United States government or Lawrence Livermore National Security, LLC. The views and opinions of authors expressed herein do not necessarily state or reflect those of the United States government or Lawrence Livermore National Security, LLC, and shall not be used for advertising or product endorsement purposes.

Explicit integrators for the time-dependent Kohn-Sham equations within the plane-wave pseudopotential formalism

André Schleife^a, Erik Draeger^b, Yosuke Kanai^{a,c,*}, Alfredo Correa^{a,*}

^aCondensed Matter and Materials Division, Lawrence Livermore National Laboratory, Livermore, CA 94550, USA

^bCenter for Applied Scientific Computing, Lawrence Livermore National Laboratory, Livermore, CA 94550, USA

^cDepartment of Chemistry, The University of North Carolina at Chapel Hill, Chapel Hill, NC 27599-3290, USA

Abstract

A comparison of explicit integrators for real-time propagation of the time-dependent Kohn-Sham equations is presented. Four algorithms are implemented and assessed for both stability and accuracy within a plane-wave pseudopotential framework, employing the adiabatic approximation to the exchange-correlation functional. Simulation results of a single sodium atom and a sodium atom embedded in bulk MgO are presented. Both the first-order Euler scheme and the second-order finite-difference scheme are found to be unstable, but it is shown that the fourth-order Runge-Kutta scheme is conditionally stable and accurate within this framework. Finally, excellent parallel scalability is demonstrated in a system of hundreds of electrons.

Keywords: time-dependent density functional theory, real-time propagation, plane-wave basis

1. Introduction

Accurately describing the quantum dynamics of electrons in numerical simulations is crucial for addressing a number of important problems in materials physics. For example, detailed understanding of the electron transfer mechanism across material interfaces is important for improving photovoltaic cells [1]. While analytical models often work reliably for describing electron transport phenomena in simple and homogeneous systems (such as organic molecules or bulk solids), quantitative simulations are necessary to accurately describe the dynamical effects of electrons in complex environments. The proper treatment of the electron dynamics is also necessary for describing highly non-equilibrium many-body electron-ion processes such as the radiation damages in materials. A variety of numerical simulations, semi-empirical [2] and *ab initio*, however, lacks the essential component: the response of the electrons to a large perturbation of the atomic coordinates. This is because the aforementioned approaches rely on the adiabatic Born-Oppenheimer approximation, i.e., on the assumption that the electrons adjust instantaneously to moving ions (e.g. by remaining in the ground state). The adiabatic Born-Oppenheimer approximation can be overcome for instance by Ehrenfest dynamics or the surface-hopping approach for a more sophisticated treatment of the electron dynamics [3].

Time-dependent density functional theory (TDDFT) is an attractive approach for describing quantum dynamics of electrons in materials because of its well-balanced accuracy and efficiency. TDDFT, as a formal extension of ground-state DFT for the treatment of time-dependent Hamiltonians, has been applied to various problems in many different areas ranging from materials science to biochemistry (see e.g. Ref. [4] and references therein). The popularity of TDDFT in various fields has led to a number of recent developments in the formal theory itself as well as in the practical aspect of implementing the theory for numerical calculations [5, 6, 7].

While the majority of applications currently exploits the linear-response formulation of TDDFT [8] to investigate the excitation of electrons based on the ground state solution of the Kohn-Sham (KS) equations, the so-called real-time

*Corresponding author

Email addresses: a.schleife@llnl.gov (André Schleife), draeger1@llnl.gov (Erik Draeger), ykanai@email.unc.edu (Yosuke Kanai), correaa@llnl.gov (Alfredo Correa)

TDDFT (RT-TDDFT) aims at explicitly obtaining the time-dependence of electronic states through the time-dependent KS Hamiltonian. Using RT-TDDFT, it is possible to compute electronic excitation spectra from the dynamics itself, in addition to investigating the quantum dynamics of electrons in real time. The RT-TDDFT approach is gaining increasing popularity as many time-dependent phenomena are becoming an important focus of modern materials research.

In this work, we numerically assess a number of explicit integrators for the time-dependent Kohn-Sham (TDKS) equations, a set of coupled non-linear partial differential equations, in TDDFT. We have built our RT-TDDFT implementation upon the Qbox code [9, 10], a highly scalable DFT code based on the plane wave pseudopotential formalism. The excellent scalability of underlying components in the code allows us to immediately apply the new method to the large heterogeneous systems needed to explore modern applications. At the same time, the plane wave basis will ensure broad applicability to a diverse set of materials as numerical convergence can be rigorously tested by systematically increasing the basis size.

The paper is structured as follows: In Sec. 2 the theoretical framework is outlined and computational details are discussed. In particular, the conservation of the energy is presented as a criterion to assess the numerical stability and accuracy of the propagators that are introduced in Sec. 3. In the following, these integrators are applied to two test systems: (i) an isolated Na atom (Sec. 4) and (ii) a 64-atom supercell containing a Na atom embedded in bulk MgO (Sec. 5). Finally, Sec. 6 summarizes the findings of this work.

2. Theoretical framework and numerical treatment

2.1. Time-dependent Kohn-Sham equations

TDDFT is based on the one-to-one correspondence between the (time-dependent) one-particle density $n(\mathbf{r}, t)$ and the (time-dependent) one-particle potential $V_{\text{ext}}(\mathbf{r}, t)$ acting on a fictitious system of non-interacting particles. This correspondence is established by the Runge-Gross theorem [11] which formally extends the Hohenberg-Kohn theorem [12]) to the time-dependent case. As a consequence of the Runge-Gross theorem, it is possible to also generalize the fictitious system of non-interacting KS particles [13] under the influence of an effective KS potential to the time-dependent case. These TDKS equations read

$$i\hbar \frac{d}{dt} |\phi_i(t)\rangle = \hat{H}(t)[n] |\phi_i(t)\rangle = \left\{ \hat{T} + \hat{V}_{\text{ext}}(t) + \hat{V}_{\text{HXC}}[n] \right\} |\phi_i(t)\rangle. \quad (1)$$

In Eq. (1), \hat{T} is the kinetic energy operator and $V_{\text{HXC}}[n](\mathbf{r}, t) = \int \frac{n(\mathbf{r}', t)}{|\mathbf{r} - \mathbf{r}'|} d\mathbf{r}' + \frac{\delta E_{\text{XC}}}{\delta n(\mathbf{r}, t)}$ is the sum of the Hartree (H) potential and the exchange-correlation (XC) potential, which is derived from a universal XC functional $E_{\text{XC}}[n]$. The electron density n follows from the occupied KS states (labeled by the index i) according to $n(\mathbf{r}, t) = \sum_i |\phi_i(\mathbf{r}, t)|^2$.

RT-TDDFT aims at obtaining the (time-dependent) solutions to the non-linear TDKS equations (1) for given initial conditions for ϕ_i . It is assumed that the so-called adiabatic functional approximation [14] (in which the XC functional depends only on the electron density at the instantaneous time) is fulfilled, i.e., $V_{\text{HXC}}[n](\mathbf{r}, t) \equiv V_{\text{HXC}}^{\text{adiab}}[n(t)](\mathbf{r}) = \frac{\partial E_{\text{HXC}}}{\partial n(\mathbf{r})}[n(t)]$. In addition, the external potentials V_{ext} studied in this work are not explicitly time dependent since they arise exclusively from the Coulomb attraction of the electrons to the ions at their *fixed* positions.

In order to solve the TDKS equations, Eq. (1), a set of initial conditions for the wave functions is necessary; in this work, they are represented by the perturbed ground-state wave functions. They are obtained by applying an additional perturbation (see below) to the solutions of the time-independent KS Hamiltonian.

2.2. Energy conservation during the propagation

The TDKS equations [cf. Eq. (1)] reduce to the KS equations in the case that the time dependence is factored out. In addition, within the adiabatic approximation they have the property to conserve the total energy $E(t)$,

$$E(t) = \sum_i \langle \phi_i(t) | \hat{T} | \phi_i(t) \rangle + \int n(\mathbf{r}, t) V_{\text{ext}}(\mathbf{r}, t) d\mathbf{r} + E_{\text{HXC}}[n](t) \quad (2)$$

which is a generalization of the time-independent KS energy [15]. For the case of HXC potentials that only depend on the instantaneous density, i.e. the adiabatic functional approximation, the conservation of the energy [16] can be seen from the total time derivative of Eq. (2),

$$\begin{aligned} \frac{dE(t)}{dt} &= \sum_i \left\{ \left\langle \phi_i(t) \left| \hat{T} \left| \frac{d}{dt} \phi_i(t) \right\rangle + \text{c.c.} \right\} \right. \\ &\quad + \sum_i \left\{ \left\langle \phi_i(t) \left| \hat{V}_{\text{ext}}(t) \left| \frac{d}{dt} \phi_i(t) \right\rangle + \text{c.c.} \right\} + \sum_i \left\{ \left\langle \phi_i(t) \left| \left(\frac{d}{dt} \hat{V}_{\text{ext}}(t) \right) \left| \phi_i(t) \right\rangle \right\} \right. \\ &\quad \left. + \frac{d}{dt} E_{\text{HXC}}[n(t)]. \right. \end{aligned} \quad (3)$$

The last term requires some attention:

$$\begin{aligned} \frac{d}{dt} E_{\text{HXC}}[n(t)] &= \int \frac{\partial E_{\text{HXC}}[n(t)]}{\partial n(\mathbf{r})} \frac{\partial n(\mathbf{r}, t)}{\partial t} d\mathbf{r} = \int V_{\text{HXC}}^{\text{adiab}}[n(t)](\mathbf{r}) \frac{\partial n(\mathbf{r}, t)}{\partial t} d\mathbf{r} \\ &= \sum_i \left\{ \left\langle \phi_i(t) \left| \hat{V}_{\text{HXC}}^{\text{adiab}}[n(t)] \left| \frac{d}{dt} \phi_i(t) \right\rangle + \text{c.c.} \right\} \right. \end{aligned} \quad (4)$$

Inserting Eq. (4) into Eq. (3) and collecting terms to recover the KS Hamiltonian we obtain:

$$\frac{d}{dt} E(t) = \sum_i \left\{ \left\langle \phi_i(t) \left| \hat{H}[n(t)] \left| \frac{d}{dt} \phi_i(t) \right\rangle + \text{c.c.} \right\} + \int n(\mathbf{r}, t) \frac{\partial V_{\text{ext}}(\mathbf{r}, t)}{\partial t} d\mathbf{r} \right. \quad (5)$$

Using the equations of motion, Eq. (1), it becomes clear [16] that the sum of the first terms in Eq. (5) is zero. The last term also vanishes if the external potential does not depend on the time t , as it is the case for the systems considered here. Energy conservation is an important property of the TDKS equations since it can be used as a test of both stability and numerical accuracy of the numerical integration of the TDKS equations.

2.3. Plane-wave expansion of the wave functions

For the numerical treatment of the TDKS equations the KS orbitals need to be expanded in a finite number of basis functions. In this work, a supercell approach with periodic boundary conditions is used and, hence, the Bloch theorem [17] can be exploited, leading to the expression

$$\phi_i(\mathbf{r}, t) = \psi_{n\mathbf{k}}(\mathbf{r}, t) = \frac{1}{\sqrt{\Omega}} e^{i\mathbf{k}\cdot\mathbf{r}} u_{n\mathbf{k}}(\mathbf{r}, t) \quad (6)$$

for the wave functions, where $u_{n\mathbf{k}}(\mathbf{r}, t)$ is a lattice-periodic function and Ω is the volume of the supercell. The indices n and \mathbf{k} label the eigenstates and the \mathbf{k} vectors in the Brillouin zone, respectively. Expanding the wave functions into plane waves as

$$\psi_{n\mathbf{k}}(\mathbf{r}, t) = \frac{1}{\sqrt{\Omega}} \sum_{\mathbf{G}} C(\mathbf{G}, t) e^{i(\mathbf{k}+\mathbf{G})\cdot\mathbf{r}} \quad (7)$$

has been quite successful in terms of numerical accuracy, convergence, and computational scalability. This basis set is orthonormal and provides an unbiased and spatially homogeneous expansion that converges numerically by systematically increasing merely a single parameter, the cutoff energy $E_{\text{cut}} = \frac{G_{\text{cut}}^2}{2}$. E_{cut} corresponds to the maximum kinetic energy of all plane waves in the calculation.

Since the basis itself is time independent, all the time dependence is carried by the plane-wave coefficients $C(\mathbf{G})$ of the expansion. This implies that the spatial partial derivatives of the wave functions are readily available in the reciprocal space. It is also useful to note that the plane waves are independent of the nuclei positions, which makes the framework convenient for first principles molecular dynamics approaches, thanks to the absence of basis set superposition errors and spurious Pulay forces [18].

2.4. Computational details

Treating the singularity of the Coulomb potential in the close vicinity of the nuclei is computationally expensive in a plane-wave basis since a very large number of basis functions is needed for converged calculations. The pseudopotential approach is used to circumvent this issue by replacing the core electrons with non-local effective potentials, which are derived by inverting the atomic KS equation (see e.g. Ref. [19]). In the present work, Hamann-Schlüter-Chiang norm-conserving pseudopotentials with a modification by D. Vanderbilt [20] are used within the Kleinman-Bylander approach [21].

The local-density approximation as parametrized by Perdew and Zunger [22] is used within the adiabatic approximation for the exchange-correlation potential in the calculations. Due to the size of the supercells in this work it is sufficient to use only the Γ point to sample the Brillouin zone even though the implementation is capable of taking \mathbf{k} points into account.

3. Propagation schemes

3.1. General considerations

For a non-interacting time-dependent Schrödinger equation (TDSE) there exists a plethora of numerical propagators to choose from. Their key properties such as (semiexact) norm conservation and (semiexact) energy conservation as well as other numerical properties including different conditions of stability (with respect to the time/space discretization) are well known [23]. For the case of the TDKS equations, Eq. (1), in combination with a plane-wave expansion of the wave functions, the situation is complicated by several factors:

First, unlike the TDSE, the TDKS equations are non-linear, and the inverse of the KS operator is not available explicitly. Thus, all methods are semi-implicit at best, i.e., implicit with respect to the linear part of the operator only.

Second, within the plane-wave framework implicit and semi-implicit methods are not feasible due to the dimension of the linear operator (number of plane waves squared) and the practical inability to invert such a large matrix explicitly. The number of plane waves in the present calculations is over 33000, and is routinely much larger for other applications. Therefore, the (semi-implicit) Crank-Nicholson scheme, even though it has been successfully used in reduced basis set local-orbital methods (e.g. [6, 24]), is not a viable option for a plane-wave implementation.

Third, conditional or unconditional stability of a time propagation algorithm in the case of the TDSE is not a guarantee of stability for the TDKS case; due to the self-consistent nature of the TDKS, there are feedback mechanisms that can worsen the stability criterion, or even make a method completely unstable when applied to the TDKS. This is a well-known phenomenon observed in studies of the non-linear extensions of the Schrödinger equation [25, 26] and will be discussed for the second-order finite-differences scheme below.

Fourth, within the plane-wave formalism it is tempting to use approximations to the linear time-evolution operator instead of approximating the differential equation by finite differences. Moreover, split-operator Trotter-like expansions exploit the fact that the kinetic energy (the local potential) part of the Hamiltonian is diagonal in reciprocal (real) space. Since these techniques can potentially benefit from very large time steps [5, 27], they have been traditionally favored in the community [4]. However, these approaches cannot be implemented straightforwardly without further algorithmic considerations because one needs to deal with the non-local part of the pseudopotential [27]. Furthermore, the Hamiltonian operator is not a constant and not known *a priori*, since it depends on the electronic states at later times (see e.g. the Magnus expansion [28] and the railway method [5]). Hence, in this work we restrict ourselves to finite-difference approximations which have a controlled order in the error.

Note also that all propagators investigated in this work rely on the application of the entire Hamiltonian to the wave function and on updating the Hamiltonian correspondingly; therefore, no particular structure of the Hamiltonian is assumed or exploited for the propagation. Consequently, for the integration of the TDKS equations we can directly take advantage of some of the existing DFT architecture as implemented in the Qbox code. This code is optimized for scalability and features highly-optimized routines for solving the regular KS equations on a large number of processors [29].

3.2. First-order Euler scheme

The Euler approach is the simplest propagation scheme in which the wave functions at the time $t + \Delta t$ are obtained from the one at time t according to

$$|\phi(t + \Delta t)\rangle = |\phi(t)\rangle - i \Delta t \hat{H}[n] |\phi(t)\rangle. \quad (8)$$

For this scheme, only the static Hamiltonian at $t = 0$ (i.e. $\hat{H}[n(t = 0) = n_0]$) is considered in this work, instead of the self-consistent (density-dependent) Hamiltonian. This is due to the numerical instability issues that we observed for this scheme and discuss below. The computational load associated with solving Eq. (8) arises from a single application of the Hamiltonian to the wave functions. The error in this scheme is $\mathcal{O}(\Delta t)$, i.e., first-order in Δt .

3.3. Second-order finite differences

Within the second-order finite-difference scheme (hereafter called the SOD scheme) more information than in the Euler scheme is used to calculate the wave functions at $t + \Delta t$ from the ones at both t and $t - \Delta t$ according to

$$|\phi(t + \Delta t)\rangle = |\phi(t - \Delta t)\rangle - 2i \Delta t \hat{H}[n] |\phi(t)\rangle. \quad (9)$$

SOD is slightly more sophisticated than the Euler approach, and the error is $\mathcal{O}(\Delta t^2)$. As in the case of the Euler scheme, the Hamiltonian has to be applied only once for each time step, but two copies of the wave functions (at t and $t - \Delta t$) need to be stored in memory for the calculation of the new wave functions.

For the propagation according to Eq. (9), three different levels of the self-consistency of the Hamiltonian [23] are compared. In the fully self-consistent approach (sc-SOD) the Hamiltonian is updated at each time step (cf. Eq. 9). For further assessing numerical stability and accuracy associated with the non-linearity, we consider two additional cases: (i) Within the non-self-consistent propagation (nsc-SOD) the Hamiltonian is kept fixed at $\hat{H}[n_0]$, as described for the Euler scheme above. (ii) In the semi-self-consistent propagation (sc100-SOD) the Hamiltonian is updated every 100 time steps, i.e., self-consistency is recovered every 100 steps.

3.4. Second-order Runge-Kutta scheme

Another second-order approach tested in this work is the second-order Runge-Kutta [30] scheme (called RK2 in the following). In this case, the wave functions at $t + \Delta t$ are computed according to

$$\begin{aligned} |k_1\rangle &= -i \Delta t \hat{H}[n_{\phi(t)}] |\phi(t)\rangle, \\ |k_2\rangle &= -i \Delta t \hat{H}[n_{\phi(t)+0.5 \cdot k_1}] |\phi(t) + 0.5 \cdot k_1\rangle, \\ |\phi(t + \Delta t)\rangle &= |\phi(t) + k_2\rangle. \end{aligned} \quad (10)$$

As with the SOD scheme, the integration error scales as $\mathcal{O}(\Delta t^2)$. The higher sophistication of this approach with respect to the Euler scheme is achieved by invoking multiple evaluations of the Hamiltonian and deriving the updated wave functions from these intermediate steps [30]. While this method allows for larger time steps for the integration of the TDKS equations, it also comes with higher computational cost due to the additional updates of the Hamiltonian and its application to the respective wave functions.

3.5. Fourth-order Runge-Kutta scheme

The fourth-order Runge-Kutta scheme (RK4) is a step beyond the RK2 method, further improved by including more intermediate evaluations of the Hamiltonian [30]. In this case, the propagation is done according to

$$\begin{aligned} |k_1\rangle &= -i \Delta t \hat{H}[n_{\phi(t)}] |\phi(t)\rangle, \\ |k_2\rangle &= -i \Delta t \hat{H}[n_{\phi(t)+0.5 \cdot k_1}] |\phi(t) + 0.5 \cdot k_1\rangle, \\ |k_3\rangle &= -i \Delta t \hat{H}[n_{\phi(t)+0.5 \cdot k_2}] |\phi(t) + 0.5 \cdot k_2\rangle, \\ |k_4\rangle &= -i \Delta t \hat{H}[n_{\phi(t)+k_3}] |\phi(t) + k_3\rangle, \\ |\phi(t + \Delta t)\rangle &= \left| \phi(t) + \frac{1}{6}k_1 + \frac{1}{3}k_2 + \frac{1}{3}k_3 + \frac{1}{6}k_4 \right\rangle. \end{aligned} \quad (11)$$

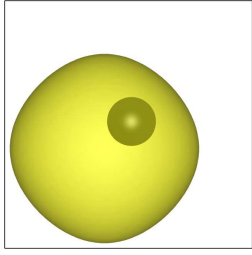


Figure 1: (Color online) Cubic unit cell containing a single Na atom (small black circle). To prepare a non-equilibrium initial condition, the Na 3s wave function (represented by the yellow isosurface) has been shifted by $(0.32, 0.32, 0.32)$ Å.

The RK4 scheme clearly shows the highest computational cost, as it requires four evaluations and updates of the Hamiltonian. On the other hand, the time step can be chosen much larger because the integration error only scales as $O(\Delta t^4)$.

4. Test case I: the isolated Na atom

As a test of the propagators introduced in Sec. 3, the time-evolution of a single Na atom in a cubic supercell ($a=7.94$ Å) is studied (cf. Fig. 1). The size of this supercell, i.e., the distance between mirror images of the Na atom, has been chosen such that the total energy does not change more than 55 meV upon a further increase of the cell size. The plane-wave cutoff energy was chosen to be 70 Ry which ensures that the total energy is converged to about 20 meV. For this system the ground-state density is calculated within DFT and, subsequently, the 3s wave function is shifted by $(0.32, 0.32, 0.32)$ Å in real space in order to prepare a non-equilibrium initial condition for the time propagation. Note that the orthogonality among the wave functions is no longer preserved after this shift which we purposely introduce for the aim of testing the different integrators.

4.1. Numerical stability and conservation of energy

The numerical stability is one of the most important criteria when solving the TDKS equations with the explicit integrators introduced above. Since the total energy is a conserved quantity, as discussed in Sec. 2.2, it is used as a measure of the stability of the propagation.

In Fig. 2 the time evolution of the total energy is shown for the different schemes introduced in the previous section. A time step of $\Delta t = (0.069$ as) is used for all schemes except for the RK4 one; in this case a ten times larger time step was used.

From Fig. 2(a) it can be seen that the Euler scheme, even though the Hamiltonian is kept fixed during the propagation, is highly unstable. The total energy diverges very quickly after a decrease from its original value. In the same figure, the results obtained using the RK2 propagator are in agreement with the RK4 propagator and it is found that they conserve the total energy within 2.72 meV for a propagation time of up to 11 fs. Even though both of the two propagation schemes appear to fulfill the numerical stability, the RK2 scheme eventually becomes unstable for a longer propagation as discussed below. For the RK4 approach, also the conservation of the norm of the unshifted wave functions was checked and found to be conserved up to within 10^{-6} during the propagation to $t = 13.8$ fs. In addition, Fig. 2(a) shows that the sc100-SOD scheme is able to maintain the stability to a certain point: Up until ≈ 8.5 fs the total energy is conserved fairly well and is only slightly smaller than the initial value. However, beyond that point the deviation grows very quickly and the total energy again diverges.

For comparison, the different levels of self-consistency in the SOD scheme as shown in Fig. 2(b) are analyzed. The figure clearly shows that the sc-SOD scheme is numerically unstable even for a propagation time of less than 0.1 fs. Keeping the Hamiltonian fixed for some number of integration steps (e.g. 100 in this work) improves the numerical stability of the algorithm, leading to a stable propagation for a much longer time [cf. Fig. 2(a)]. The nsc-SOD scheme is found to be conditionally stable, however, keeping the Hamiltonian fixed is unphysical for practical applications within RT-TDDFT. Therefore, the SOD schemes are an example of an explicit method that is well-behaved in the non-self-consistent case (nsc-SOD or, for instance, the linear Schrödinger equation) but becomes unconditionally unstable

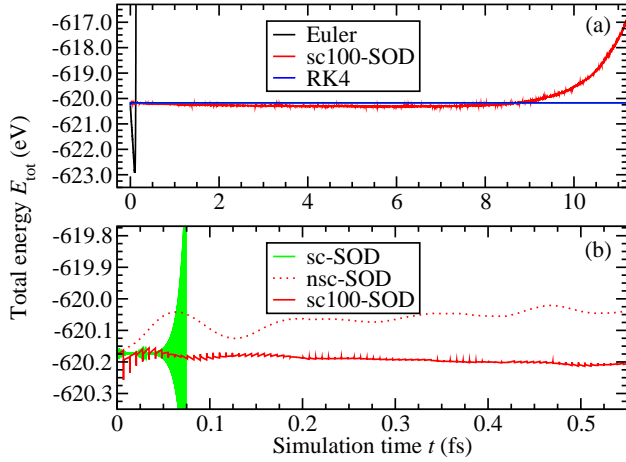


Figure 2: (Color online) Total energy E_{tot} (in eV) of the Na atom (at $t = 0$ fs the $3s$ wave function was shifted by $(0.32, 0.32, 0.32)$ Å from its equilibrium position in real space) as a function of time t (in fs). In (a) the Euler scheme (black solid line, $\Delta t = 0.069$ as) and the sc100-SOD second-order finite-difference scheme (red solid line, $\Delta t = 0.069$ as) are compared to the Runge-Kutta propagators (blue solid line). The second-order ($\Delta t = 0.069$ as) and the fourth-order ($\Delta t = 0.691$ as) Runge-Kutta scheme yield the same trajectory for the times shown in (a). In (b) the fully self-consistent second-order finite-difference method (green solid line) is compared to the sc100-SOD (red solid line) and the non-self-consistent (red dotted line) one for $\Delta t = 0.069$ as.

for the integration of the self-consistent TDKS. This illustrates the difficulty of having to deal with the non-linear Hamiltonian of the TDKS formalism when the time propagation is performed.

For investigating further details, Fig. 3 shows the numerical stability of the RK2 (the sc100-SOD second-order) propagation schemes up to 35 fs (11 fs) as calculated using different time steps Δt . For both propagators, the propagation becomes expeditiously more stable when smaller time steps are used. In addition, from comparing Fig. 3(a) and (b) it is found that the (fully self-consistent) RK2 scheme is much more stable than the sc100-SOD when the same time step is chosen. The total energy deviations in the stable regime are also much smaller for the RK2 case.

As mentioned earlier, the nsc-SOD and the RK4 propagator are found to be conditionally stable in this work, i.e., they can be used for propagation of arbitrary duration as long as the time step Δt is chosen to be small enough. Plotting the critical time step (for which the propagation is numerically found to remain stable) versus the plane-wave cutoff energy E_{cut} in Fig. 4 indicates an inverse proportionality of Δt and E_{cut} . Furthermore, it can be seen that the critical time step used in the RK4 scheme can be roughly three times as large as the one used in the nsc-SOD for a given E_{cut} . We emphasize, however, that the nsc-SOD scheme is not physically meaningful for propagating the TDKS equation even though it is numerically robust.

4.2. Evolution of the system

In order to illustrate the evolution of the system during the propagation, the total energy, being a conserved quantity, does not provide helpful insights. Instead, the sum of the expectation values, $\sum_i \langle \phi_i(t) | \hat{H}[n] | \phi_i(t) \rangle$, as shown in Fig. 5 is used as a time dependent quantity that provides qualitative information of the energy spectrum of the wave functions. As expected, the results from the Euler scheme are not useful due to the immediate instability of this propagation scheme. For t up to ≈ 13 fs it can be seen in Fig. 5(a) that the RK2 and RK4 propagations agree with each other exactly (therefore only RK4 is shown) even though they are calculated using different Δt . They show pronounced oscillations with a period of approximately 1.5 fs. Additionally, contributions from other higher frequencies become visible from the fine structure of the curves. These features derive from the fact that the wave function that was shifted at $t = 0$ starts to oscillate around the (fixed) position of the nucleus, as expected. Also other wave functions start to oscillate through the self-consistent potential (which depends on all occupied wave functions) in the TDKS Hamiltonian.

We note that test calculations have shown that varying the plane-wave cutoff energy between 50 Ry and 80 Ry does not significantly impact the time evolution of the system with the change in the sum of the expectation values remaining smaller than 8 meV.

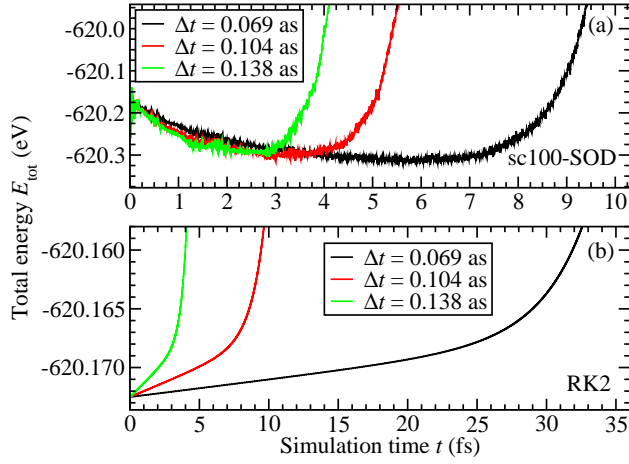


Figure 3: (Color online) Total energy E_{tot} (in eV) of the Na atom as a function of time t (in fs). The curves in (a) result from the sc100-SOD second-order finite-difference scheme and the ones in (b) from the second-order Runge-Kutta scheme. Time steps of $\Delta t = 0.069$ as (black solid lines), $\Delta t = 0.104$ as (red solid lines), and $\Delta t = 0.138$ as (green solid lines) were used.

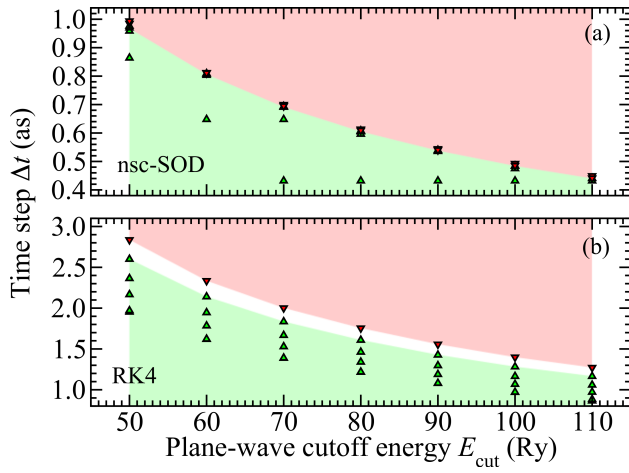


Figure 4: (Color online) Time steps Δt (in as) for which the non-self-consistent second-order finite-difference scheme (a) or the fourth-order Runge-Kutta scheme (b) are stable (green triangles pointing up) or unstable (red triangles pointing down), depending on the respective plane-wave cutoff energy E_{cut} (in Ry) used.

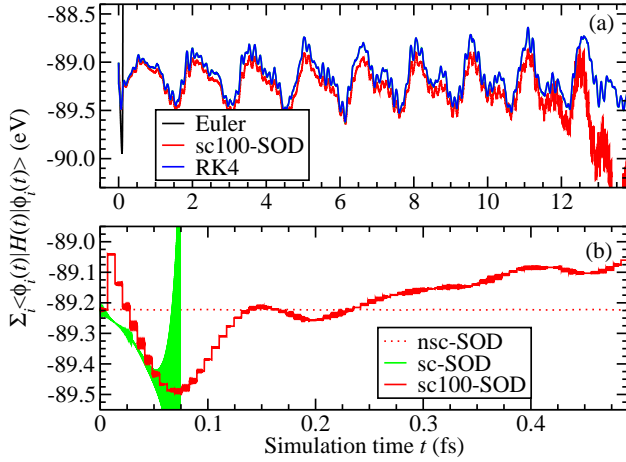


Figure 5: (Color online) Sum of the expectation values $\sum_i \langle \phi_i(t) | \hat{H}[n] | \phi_i(t) \rangle$ (in eV) of all valence wave functions i of the Na atom (at $t = 0$ fs the $3s$ wave function was shifted by $(0.32, 0.32, 0.32)$ Å from its equilibrium position in real space) as a function of time t (in fs). In (a) the Euler scheme (black solid line, $\Delta t = 0.069$ as) and the sc100-SOD second-order finite-difference scheme (red solid line, $\Delta t = 0.069$ as) are compared to the Runge-Kutta propagators (blue solid line). The second-order ($\Delta t = 0.069$ as) and the fourth-order ($\Delta t = 0.691$ as) Runge-Kutta scheme yield the same trajectory for the times shown in (a). In (b) the fully self-consistent second-order finite-difference method (green solid line) is compared to the sc100-SOD (red solid line) and the non-self-consistent (red dotted line) one for $\Delta t = 0.069$ as.

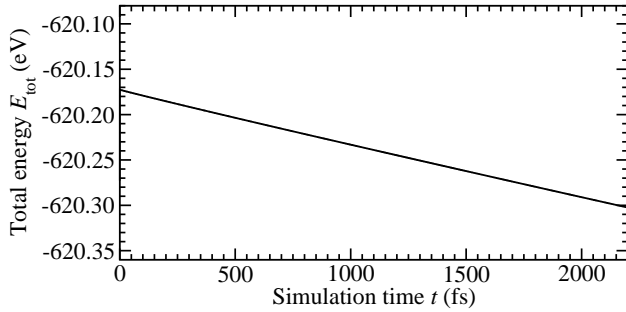


Figure 6: (Color online) Total energy E_{tot} (in eV) of the Na atom (at $t = 0$ fs the $3s$ wave function was shifted by $(0.32, 0.32, 0.32)$ Å from its equilibrium position in real space) as a function of time t (in fs). The results have been obtained using the RK4 propagator and $\Delta t = 0.691$ as.

Comparing the results of the two Runge-Kutta propagators [cf. Fig. 5(a)] to the behavior obtained using the sc100-SOD propagation scheme shows a close similarity for small times t . However, this agreement becomes worse for larger times, i.e., when the sc100-SOD becomes increasingly unstable. In accordance with the discussion of the total energy, Fig. 5(b) points out that the sc-SOD becomes unstable and, hence, does not yield meaningful results for the expectation-value sum for $t > 0.1$ fs. Even though the nsc-SOD is conditionally stable, Fig. 5(b) shows that the expectation-value sum does not change during the propagation because of the non-self-consistent nature of the propagation.

Figure 6 shows the long-term stability of the propagation using the RK4 scheme; the total energy for the Na atom is plotted for a total propagation time of 2.2 ps. It can be seen that the total energy is well conserved during the propagation with a deviation of less than 30 meV during the 2.2 ps. As discussed above, the integration error in the RK4 scheme scales as $O(\Delta t^4)$. More specifically, it has been found numerically that the total energy conservation (per unit time) can be improved by a factor of 27.8 when the time step is reduced by a half.

5. Test case II: Na atom embedded in MgO

Having established that the RK4 method is suitable for our implementation of RT-TDDFT within a plane-wave pseudopotential formalism, we now show that the scheme is suitable for investigating large, complex systems. We

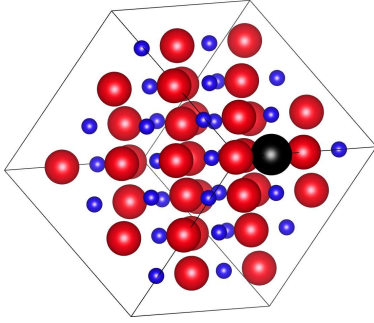


Figure 7: (Color online) The 64-atom unit cell of MgO (Mg atoms red circles, O atoms blue circles) containing a single Na atom (black circle) on an oxygen lattice position.

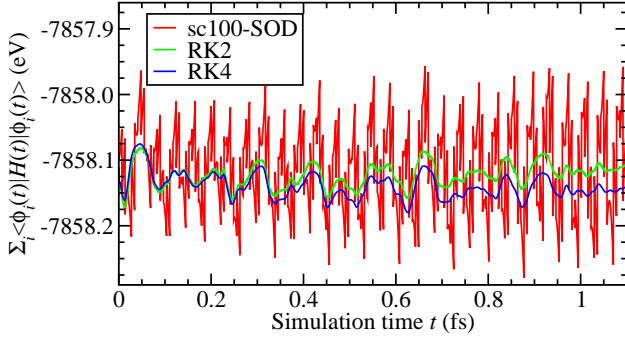


Figure 8: (Color online) Sum of the expectation values $\sum_i \langle \phi_i(t) | \hat{H}[n] | \phi_i(t) \rangle$ (in eV) of all valence wave functions in the Na:MgO 64-atom supercell (at $t = 0$ fs the Na-induced level within the MgO gap was shifted by (0.032, 0.032, 0.032) Å from its equilibrium position in real space) as a function of time t (in fs). The sc100-SOD second-order finite-difference scheme (red solid line, $\Delta t = 0.069$ as) is compared to the second-order (green solid line, $\Delta t = 0.069$ as) and the fourth-order (blue solid line, $\Delta t = 0.691$ as) Runge-Kutta scheme.

applied our implementation to a bulk system, consisting of a 64-atom supercell of crystalline MgO with one of the O atoms replaced by a Na atom. This corresponds to 32 Mg atoms, 31 O atoms, and 1 Na atom with a total of 449 electrons in the calculation (cf. Fig. 7). After obtaining the ground state of the system, the 3s wave function of the Na atom is shifted by (0.032, 0.032, 0.032) Å in real space to obtain a non-equilibrium initial condition for the time propagation.

The evolution of the Na:MgO system is shown in Fig. 8 using again the sum of the expectation values as an example for a quantity of interest. The sc100-SOD and the RK2 are also shown for comparison to the RK4 propagation scheme. The intrinsic inaccuracy of the sc100-SOD scheme is evident in the figure as this propagator is applied to a complex system such as Na:MgO: the oscillations are much too large and the long time stability is worse, as discussed earlier.

To test the long-term stability of the RK4 propagation also for this complex system, we plotted the total energy for a total propagation time of 118 fs in Fig. 9. The total energy is well-conserved during the propagation; the deviation remains on the order of 2.7 eV during 118 fs. Note that this error corresponds to merely 0.006 % of the total energy of the system, hence, the magnitude of the deviation per electron is on the same order as in the case of a single Na atom. Furthermore, as discussed above it can be reduced by a factor of ≈ 28 by using a half of the time step size.

5.1. Parallel scaling

Finally, it is important to analyze the scaling of the RT-TDDFT implementation presented in this work with respect to the number of processor cores the calculation is run on. In Fig. 10 the time required to perform one step of steepest descent (SD), which is a typical method for obtaining solutions to the ground-state Hamiltonian, is compared to the time required to perform one step of real time propagation using the RK4 method. The RK4 method requires four updates of the Hamiltonian and four evaluations of $\hat{H}[n_{\phi(t)}] |\phi(t)\rangle$ per time step. The SD method requires one evaluation

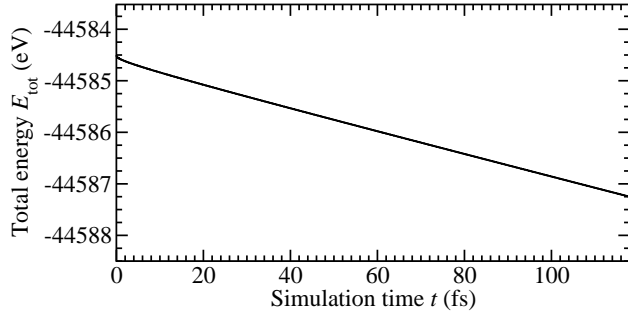


Figure 9: (Color online) Total energy E_{tot} (in eV) of the Na:MgO 64-atom supercell (at $t = 0$ fs the Na-induced level within the MgO gap was shifted by (0.032, 0.032, 0.032) Å from its equilibrium position in real space) as a function of time t (in fs). The results have been obtained using the fourth-order Runge-Kutta propagator and $\Delta t = 0.691$ as.

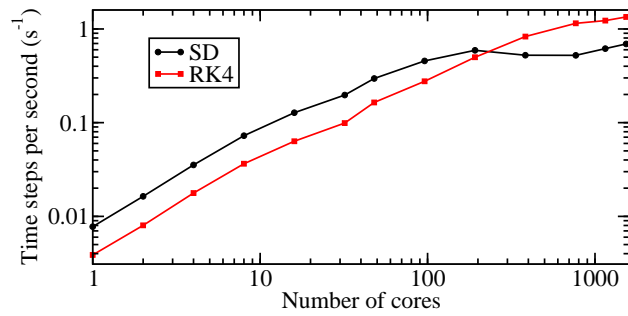


Figure 10: (Color online) The number of steps that can be performed within one second wall time is plotted versus the number of processing cores used in the calculation for the Na:MgO 64-atom supercell. The steepest descent algorithm (black curve) is compared to the RK4 propagation (red curve).

of the Hamiltonian per step as well as the re-orthogonalization of the states. For that reason, the SD scheme is roughly a factor of four faster when the calculation is run on one core only.

However, the orthogonalization of the wave functions does not scale well with the number of processing cores. This becomes obvious in Fig. 10 for more than 200 cores, where the scalability of the SD scheme is significantly reduced. In contrast, the RK4 propagator scales very well (close to linearly) up to at least 1536 cores (1 step/s), benefiting directly from the highly parallelized routines in the Qbox code that are exploited for this explicit-integration scheme.

6. Conclusions

We find that the 4th order Runge-Kutta scheme is a conditionally stable and well-balanced general purpose propagator for the TDKS equations when implemented within the plane wave pseudopotential formalism. Several other integrators such as Euler scheme, the second-order finite-differences scheme, and the second-order Runge-Kutta scheme were also studied in this work. The Euler scheme was found to be highly unstable. Relaxing the self-consistency requirement of the non-linear Hamiltonian in the TDKS improves the stability of the the second-order finite differences scheme. This observation indicates that the integrators that are designed for time-dependent Schrödinger equations are not necessarily suitable for integrating TDKS equations. In limited instances, the second-order Runge-Kutta scheme can be an efficient alternative propagator (with smaller computational expense than the fourth-order version) for cases where the time step needs to be very small and the total propagation time required is not long. This can be the case for certain applications involving very fast external perturbations where the physics of the problem requires a very fine time resolution.

The explicit propagators allow for a better scalability with respect to the number of computing cores compared to typical ground-state or Born-Oppenheimer methods. The improvement results from the fact that the time-propagation schemes do not require the orthogonalization of the propagated wave functions, which is a known bottleneck for the scalability [9]. Furthermore, these explicit integrators do not assume a particular form of the potential (including the pseudopotential and exchange-correlation potential) and they can directly benefit from existing highly parallel routines developed for the Born-Oppenheimer calculations.

The present implementation of real-time TDDFT in the plane-wave pseudopotential formalism using the explicit integrators provides an ideal framework for further work in the context of first principles molecular dynamics simulations where the Born-Oppenheimer approximation is a key limitation.

Acknowledgments

We gratefully acknowledge fruitful discussions with E. K. U. Gross, A. Rubio, K. Burke, N. Maitra, and J. Kohanoff. A.S. is supported through the Physical and Life Sciences Directorate at Lawrence Livermore National Laboratory. Computing support for this work came from the Lawrence Livermore National Laboratory (LLNL) Institutional Computing Grand Challenge program. Part of this work was performed under the auspices of the U.S. Department of Energy at Lawrence Livermore National Laboratory under Contract DE-AC52-07A27344.

References

- [1] Y. Kanai, Z. Wu, J. C. Grossman, Charge separation in nanoscale photovoltaic materials: recent insights from first-principles electronic structure theory, *J. Mater. Chem.* 20 (2010) 1053–1061. doi:10.1039/B913277P.
- [2] A. Caro, M. Victoria, Ion-electron interaction in molecular-dynamics cascades, *Phys. Rev. A* 40 (1989) 2287–2291. doi:10.1103/PhysRevA.40.2287.
- [3] J. C. Tully, in: D. L. Thompson (Ed.), *Modern Methods for Multidimensional Dynamics Computations in Chemistry*, World Scientific, 1998.
- [4] M. Marques, E. Gross, Time-dependent density functional theory, *Annu. Rev. Phys. Chem.* 55 (2004) 427–455.
- [5] O. Sugino, Y. Miyamoto, Density-functional approach to electron dynamics: Stable simulation under a self-consistent field, *Phys. Rev. B* 59 (1999) 2579–2586. doi:10.1103/PhysRevB.59.2579.
- [6] A. Castro, M. A. L. Marques, A. Rubio, Propagators for the time-dependent kohn-sham equations 121 (8) (2004) 3425–3433. doi:10.1063/1.1774980.
- [7] A. Castro, M. Marques, Propagators for the time-dependent kohn-sham equations, in: M. Marques, C. Ullrich, F. Nogueira, A. Rubio, K. Burke, E. Gross (Eds.), *Time-Dependent Density Functional Theory*, Vol. 706 of *Lecture Notes in Physics*, Springer Berlin / Heidelberg, 2006, pp. 197–210. doi:10.1007/3-540-35426-3_12.

- [8] M. Casida, Time-dependent density-functional response theory for molecules, in: C. D. P. (Ed.), *Recent Advances in Density Functional Methods, Part I*, World Scientific / Singapore, 1995, p. 155.
- [9] F. Gygi, Architecture of qbox: A scalable first-principles molecular dynamics code, *IBM Journal of Research and Development* 52 (1.2) (2008) 137–144.
- [10] F. Gygi, R. Yates, J. Lorenz, E. Draeger, F. Franchetti, C. Ueberhuber, B. de Supinski, S. Kral, J. Gunnels, J. Sexton, Large-scale first-principles molecular dynamics simulations on the bluegene/l platform using the qbox code, in: *Supercomputing, 2005. Proceedings of the ACM/IEEE SC 2005 Conference*, IEEE Computer Society, 2005, p. 24. doi:10.1109/SC.2005.40.
- [11] E. Runge, E. K. U. Gross, Density-functional theory for time-dependent systems, *Phys. Rev. Lett.* 52 (1984) 997–1000. doi:10.1103/PhysRevLett.52.997.
- [12] P. Hohenberg, W. Kohn, Inhomogeneous electron gas, *Phys. Rev.* 136 (3B) (1964) B864–B871. doi:10.1103/PhysRev.136.B864.
- [13] W. Kohn, L. J. Sham, Self-consistent equations including exchange and correlation effects, *Phys. Rev.* 140 (4A) (1965) A1133–A1138. doi:10.1103/PhysRev.140.A1133.
- [14] E. K. U. Gross, F. J. Dobson, M. Petersilka, *Density Functional Theory*, Springer, New York, NY, USA, 1996.
- [15] R. M. Martin, *Electronic Structure: Basic Theory and Practical Methods* (v. 1), 1st Edition, Cambridge University Press, 2008.
- [16] E. K. U. Gross, private communication (2011).
- [17] F. Bloch, Über die quantenmechanik der elektronen in kristallgittern, *Z. Phys. A* 52 (7–8) (1929) 555. doi:10.1007/BF01339455.
- [18] P. Pulay, Ab initio calculation of force constants and equilibrium geometries in polyatomic molecules, *Mol. Phys.* 17 (2) (1969) 197–204. doi:10.1080/00268976900100941.
- [19] M. Fuchs, M. Scheffler, Ab initio pseudopotentials for electronic structure calculations of poly-atomic systems using density-functional theory, *Comput. Phys. Commun.* 119 (1) (1999) 67–98. doi:10.1016/S0010-4655(98)00201-X.
- [20] D. Vanderbilt, Optimally smooth norm-conserving pseudopotentials, *Phys. Rev. B* 32 (1985) 8412–8415. doi:10.1103/PhysRevB.32.8412.
- [21] L. Kleinman, D. M. Bylander, Efficacious form for model pseudopotentials, *Phys. Rev. Lett.* 48 (1982) 1425–1428. doi:10.1103/PhysRevLett.48.1425.
- [22] J. P. Perdew, A. Zunger, Self-interaction correction to density-functional approximations for many-electron systems 23 (10) (1981) 5048–5079. doi:10.1103/PhysRevB.23.5048.
- [23] C. Leforestier, R. H. Bisseling, C. Cerjan, M. D. Feit, R. Friesner, A. Guldberg, A. Hammerich, G. Jolicard, W. Karrlein, H. D. Meyer, N. Lipkin, O. Roncero, R. Kosloff, A comparison of different propagation schemes for the time dependent Schrödinger equation, *J. Comput. Phys.* 94 (1) (1991) 59–80. doi:10.1016/0021-9991(91)90137-A.
- [24] J. M. Soler, E. Artacho, J. D. Gale, A. García, J. Junquera, P. Ordejón, D. Sánchez-Portal, The siesta method for ab initio order- n materials simulation, *J. Phys. Condens. Mat.* 14 (11) (2002) 2745. doi:10.1088/0953-8984/14/11/302.
- [25] W. Bao, D. Jaksch, An explicit unconditionally stable numerical method for solving damped nonlinear schrödinger equations with a focusing nonlinearity, *SIAM J. Numer. Anal.* 41 (4) (2004) 1406–1426.
URL <http://www.jstor.org/stable/4101176>
- [26] P. A. Ruprecht, M. J. Holland, K. Burnett, M. Edwards, Time-dependent solution of the nonlinear schrödinger equation for bose-condensed trapped neutral atoms, *Phys. Rev. A* 51 (1995) 4704–4711. doi:10.1103/PhysRevA.51.4704.
- [27] O. Sugino, Y. Miyamoto, Time-dependent density functional molecular dynamics simulation, *RIKEN Review* (2000) 47–48.
- [28] W. Magnus, On the exponential solution of differential equations for a linear operator, *Commun. Pur. Appl. Math.* 7 (4) (1954) 649–673. doi:10.1002/cpa.3160070404.
- [29] F. Gygi, E. W. Draeger, M. Schulz, B. R. de Supinski, J. A. Gunnels, V. Austel, J. C. Sexton, F. Franchetti, S. Kral, C. W. Ueberhuber, J. Lorenz, Large-scale electronic structure calculations of high-z metals on the bluegene/l platform, in: *Proceedings of the 2006 ACM/IEEE conference on Supercomputing, SC '06*, ACM, New York, NY, USA, 2006. doi:10.1145/1188455.1188502.
- [30] W. H. Press, S. A. Teukolsky, W. T. Vetterling, B. P. Flannery, *Numerical Recipes 3rd Edition: The Art of Scientific Computing*, 3rd Edition, Cambridge University Press, New York, NY, USA, 2007.